Interaction between El Niño and Extreme Indian Ocean Dipole

JING-JIA LUO, RUOCHAO ZHANG AND SWADHIN K. BEHERA

Frontier Research Center for Global Change, JAMSTEC, Yokohama, Japan

YUKIO MASUMOTO

Department of Earth and Planetary Science, The University of Tokyo, Tokyo, and Frontier Research Center for Global Change, JAMSTEC, Yokohama, Japan

FEI-FEI JIN

Department of Meteorology, University of Hawaii at Mānoa, Honolulu, USA

ROGER LUKAS

Department of Oceanography, University of Hawaii at Mānoa, Honolulu, USA

TOSHIO YAMAGATA

Department of Earth and Planetary Science, The University of Tokyo, Tokyo, and Frontier Research Center for Global Change, JAMSTEC, Yokohama, Japan

J. Climate (*Submitted: 23 February 2009; 1st revision: 12 June 2009; accepted: 14 August 2009*)

Corresponding author address: Jing-Jia Luo, Research Institute for Global Change, JAMSTEC, 3173-25 Showa-machi, Kanazawa-ku, Yokohama, Kanagawa 236-0001, Japan.

E-mail: luo@jamstec.go.jp; Tel: +81-45-778-5513; Fax: +81-45-778-5707.

ABSTRACT

Climate variability in the tropical Indo-Pacific sector has undergone dramatic changes under global ocean warming. Extreme Indian Ocean Dipole (IOD) events occurred repeatedly in recent decades with unprecedented three consecutive episodes during 2006-2008, causing vast climate and socio-economic impact worldwide and weakening the historic El Niño-Indian monsoon relationship. Major attention has been paid to El Niño influence on the Indian Ocean, but how the IOD influences El Niño and its predictability remained an important issue to be understood. On the basis of various forecast experiments by activating and suppressing air-sea coupling in the individual tropical ocean basins using a state-of-the-art coupled ocean-atmosphere model with demonstrated predictive capability, the present study shows that the extreme IOD plays a key role in driving the 1994 pseudo-El Niño, in contrast with traditional El Niño theory. The pseudo-El Niño is more frequently observed in recent decades, coincident with a weakened atmospheric Walker circulation in response to anthropogenic forcing. Our results suggest that extreme IOD may significantly enhance El Niño and its onset forecast that has being a long-standing challenge and El Niño in turn enhances IOD and its long-range predictability. The intrinsic El Niño-IOD interaction found here provides a hope for enhanced prediction skill of the both and sheds new light on the tropical climate variations and their changes under global warming.

1. Introduction

El Niño and extreme Indian Ocean Dipole (IOD) are two dominant drivers for year-to-year climate variability on Earth. Predicting those climate modes is of great value because of their large environmental and societal impacts, globally and regionally. El Niño is now generally predictable at a lead time of several seasons (e.g., Palmer et al. 2004; Luo et al. 2005b; Sara et al. 2006; Jin et al. 2008) and may be predicted even up to two years in advance for specific events (Chen et al. 2004; Luo et al. 2008a). However, predicting the exact onset of El Niño remains a long-standing challenge, for either the strongest 1997-98 episode or the recent weak-to-moderate 2006-07 event (e.g., Barnston et al. 1999; Landsea and Knaff 2000; McPhaden 2006; see also the real time multi-model ENSO forecasts at http://iri.columbia.edu/climate/ENSO/currentinfo/QuickLook.html). This is consistent with the observational finding (e.g., Kessler 2002); unlike its La Niña counterpart, El Niño onset does not follow the theoretical self-sustained oscillatory behavior (e.g., Jin 1997; Neelin et al. 1998). External forcing is often necessary to initiate El Niño onsets.

Considerable observational, model and theoretical efforts were made to understand the influences of intraseasonal disturbances, especially westerly wind bursts in the equatorial western Pacific, on the El Niño onset and growth (e.g., McPhaden 1999; Fedorov et al. 2003; Gebbie et al. 2007). The importance of stochastic forcing was recognized particularly after monitoring the evolution of the very strong 1997-98 El Niño in which westerly wind bursts apparently contributed to its rapid development (e.g., McPhaden 1999; see also the Pacific TAO-TRITON buoy observations at http://www.pmel.noaa.gov/tao/jsdisplay/). The

unpredictable intraseasonal wind forcing, however, was believed to impose a fundamental limit to El Niño predictability (e.g., Flügel et al. 2004); a pessimistic result for El Niño forecasters. Recent model studies suggested that the Indian Ocean climate variability might have important influence on the Pacific El Niño-Southern Oscillation (ENSO) variance and frequency (e.g., Yu et al. 2002; Wu and Kirtman 2004; Behera et al. 2006), though their results appear to be inconsistent and model-dependent. Under certain circumstances, surface wind anomalies in the western Pacific related to the Indian Ocean basin-wide cooling or warming, as a delayed response to La Niña or El Niño, may in turn affect El Niño onset or decay during specific seasons (e.g., Kug et al. 2005 and 2006). Potential contribution of just this type of Indian Ocean signal to ENSO predictability, however, appears to be limited since the source for the predictability of the former is essentially determined by ENSO itself.

In addition to the basin-wide signal forced by ENSO predominantly through a fast atmospheric Walker circulation adjustment (e.g., Klein et al. 1999), internal air-sea coupling in the tropical Indian Ocean generates another important climate mode, called IOD (e.g., Saji et al. 1999; Webster et al. 1999). Extreme IOD events characterized by strong cooling in the eastern Indian Ocean can induce large convective diabatic heating anomalies and therefore affect the equatorial atmospheric Walker circulation and ENSO evolution. El Niño and IOD repeatedly co-occurred in recent observations since the mid-1970s (e.g., Annamalai et al. 2005), indicating the interactive nature of the two major climate modes. We note that, unlike the ENSO-induced basin-wide signal in the Indian Ocean, IOD has its own dynamics and independent source for its predictability (e.g.,

Behera et al. 2006; Luo et al. 2007 and 2008b). Thus, exploring the IOD influence on El Niño would provide additional space for our better understanding and prediction of El Niño.

In this study, we examine potential contributions of the Indo-Pacific inter-basin coupling to the predictions of both El Niño and extreme IOD, in particular their onsets. This is not just because both climate modes have large climate and socioeconomic impacts worldwide and hence enormous societal benefits from their predictions. Improved prediction of either mode could enhance the predictive skill of the other in terms of their interacting feedbacks. By conducting various forecast experiments with a fully coupled global ocean-atmosphere model, we demonstrate that extreme IOD has important influence on El Niño and its predictability, and vise versa. Thus the inter-basin coupling via the atmospheric Walker circulation is crucial to both El Niño and IOD evolutions and predictions. The coupled model and seasonal prediction experiments are described in section 2. Retrospective forecast and "perfect model" prediction results for both El Niño and extreme IOD are presented in sections 3 and 4. Summary and discussions are given in section 5.

2. Model, retrospective forecasts, and "perfect model" predictions

a. The model

The numerical model used in present study is the SINTEX-F fully coupled global ocean-atmosphere general circulation model (Luo et al. 2003 and 2005a; Masson et al. 2005), which was developed at Frontier Research Center for Global Change under the European

Union-Japan collaboration (Gualdi et al. 2003; Guilyardi et al. 2003). The atmospheric component (ECHAM4.6) has the resolution of 1.1° × 1.1° (T106) with 19 vertical levels (Roeckner et al. 1996). The oceanic component (OPA8) has a relatively coarse resolution with a 2° Mercator horizontal mesh and 31 layers in vertical (Madec et al. 1998). Its meridional resolution was increased to 0.5° near the equator in order to properly capture the equatorial wave dynamics. Those two components are coupled every two hours without any flux corrections using a standardized interface (Valcke et al. 2000). The SINTEX-F model has been applied to various climate studies and shown good performance in simulating and predicting both ENSO and IOD (e.g., Yamagata et al. 2004; Luo et al. 2005a,b; Behera et al. 2005 and 2006; Luo et al. 2007 and 2008a,b; Jin et al. 2008). Here, we refer to IOD as its positive phase (strong cooling in the eastern Indian Ocean and weak warming in the west). We note that a large asymmetry exists between the surface warming and cooling intensity in the eastern Indian Ocean associated with the negative and positive IOD events (Hong et al. 2008a,b). Negative IOD events do not appear to evolve into strong air-sea coupled processes in the Indian Ocean, and therefore their peak magnitudes are weak with lower predictability in general (Luo et al. 2007).

b. Retrospective forecast experiments

9-member ensemble retrospective forecasts for 12 target months from the first day of each month during 1982-2006 were performed based on a semi-multimodel ensemble approach; both model coupling physics and initial conditions were perturbed separately in three

different ways (see Luo et al. 2005b and 2007 for detailed descriptions). A simple but effective way was adopted to produce realistic and well-balanced ocean-atmosphere initial conditions by assimilating only satellite observed sea surface temperatures (SSTs) into the coupled model (Luo et al. 2005b). The well-balanced initial conditions are important to achieving skillful long-lead ENSO prediction out to 2 years ahead (Chen et al. 2004; Luo et al. 2008a). Interannaul oceanic thermocline variations in the equatorial Pacific, the source of memory on which useful seasonal predictions of ENSO could be based, were reproduced well in general using the coupled SST-nudging initialization approach (see Luo et al. 2005b and 2007). However, significant errors exist for specific seasons (compare left and right panels in Fig. 1), particularly when intraseasonal Kelvin waves passed. This suggests the importance of assimilating oceanic subsurface information to improving the model initial conditions. The same model initial conditions for the retrospective forecasts were used for the two sensitivity forecast experiments described below.

The east-west Walker circulation in the equatorial atmosphere, particularly the easterly (westerly) trade winds in the Pacific (Indian Ocean) driven by the strong convection over the warm waters in the Maritime Continent-western Pacific, could be regulated by and play an important role in redistribution of the warm waters in the Indo-Pacific region, in association with ENSO and IOD evolution. Influence of the inter-basin coupling on the predictions of El Niño and extreme IOD was examined by suppressing air-sea coupling in the tropical Indian Ocean (hereafter referred to as dIO) and Pacific Ocean (dPO), respectively. Monthly mean climatological SSTs, based on the satellite observations during 1983-2006 (Reynolds et al. 2002), were prescribed in the individual ocean basins between

25°S and 25°N.[1] By doing this over the basin without air-sea coupling, the atmosphere there will respond to the climatological observed SST, rather than predicted SST, during the 12-month forecast period. That is, oceanic feedbacks to the atmosphere there are suppressed, and thereby the interacting feedbacks between the Indian Ocean and Pacific SST variations via the atmospheric bridge (particularly the Walker circulation) are suppressed.[2]

c. "Perfect model" prediction experiments

We first integrated the free coupled model for 520 years, starting from Levitus annual mean climatology without motion (Luo et al. 2005a). The first 20 years had a rapid spin-up in global mean SST and thus were discarded. Within the remaining 500-year simulation, 25 co-occurrences of El Niño and extreme IOD events occurred. Consistent with the observational definitions, El Niño in the model was defined when the boreal winter

[1] A "sponge layer" of 10° width in longitude and 5° in latitude, where weights of the free air-sea coupling increase linearly toward the outside ocean, was applied in order to avoid unrealistic instability near the boundary. Climate variations in the South China Sea, influenced by and may in turn influence ENSO and IOD, were not suppressed in present study (see also Behera et al. 2006 for the free coupled model sensitivity experiments).

[2] We note that another inter-basin connection through relatively slow oceanic process, especially the Indonesia Throughflow, may also play a non-negligible role (e.g., Meyers 1996), an interesting issue to be examined further.

(December-February) mean SST anomaly in the Niño3.4 region (5°S-5°N, 120°-170°W) exceeds 0.5°C. An average SST anomaly lower than -1°C in the eastern Indian Ocean (EIO, 10°S-0°, 90°-110°E) during September to November was used as the criterion for the extreme IOD definition.

In order to assess the inter-basin coupling effects on the El Niño and extreme IOD predictions, the same air-sea decoupling approach was adopted except that the 500-year climatological model SST was prescribed in the decoupled basins. The same initial conditions produced by the free coupled model simulation were used in the two "perfect model" experiments for predicting each of the 25 El Niño and extreme IOD events. The predictions were conducted in the same manner as done in the retrospective forecast experiments for 12 target months starting from the first day of each month during July of the year before the onsets of El Niño and IOD to December of the year when the El Niño and IOD co-occurred.

3. Retrospective forecast results

a. Influence of extreme IOD on El Niño

Over last two decades, one pseudo-El Niño in 1994 and two El Niño in 1997 and 2006 appeared concurrently with extreme IOD. This combination caused severe climate impacts over the globe including the exacerbated drought in Southeast Asia-Australia and floods in

East Africa in 1994 and 2006. Figure 2 shows our model retrospective forecasts of the three El Niño with and without the Indian Ocean influence (see section 2b for the methods). Apparently, predictions of these El Niño onsets appear to completely fail in the latter case (compare the left and right panels in Fig. 2). The pseudo-El Niño in 1994-95 is characterized by major surface warming in the central Pacific rather than in the east during canonical El Niño years. Because of this, its associated global climate impacts were found to be distinct from those of typical El Niño (e.g., Weng et al. 2007). The warming in the central Pacific was also found to be more effective in forcing drought over India and Australia (Kumar et al. 2006; Wang and Hendon 2007). Interestingly, along the equatorial Pacific thermocline, no significant warm signal preceded its onset in October 1994 except a weak and shallow warming confined in the central area (see Fig. 1, top panels). This suggests the necessity of external forcing for its growth. The extreme IOD event started early in 1994 appears to have suppressed the development of a La Niña signal in the eastern Pacific and played a key role in driving the evolution of this pseudo-El Niño (the green and orange lines in Figs. 2a and 2b, see also Fig. 4a).[3]

[3] We note that, using a simple two-predictor regression model based on the equatorial Pacific warm water volume and the Madden-Julian Oscillation forcing in the western Pacific, McPhaden et al. (2006) achieved good skill in predicting most of ENSO events during 1981-2005. This linear model, however, completely failed to predict the pseudo-El Niño in1994-95 (see their Figure 3). This appears to support our finding here.

The SINTEX-F model shows a limited success in predicting the 1997-98 El Niño onset (Fig. 2c, green lines), despite the substantial influence of the unpredictable intraseasonal westerly wind bursts from late 1996 to early 1997 (e.g., McPhaden 1999; see also the Pacific TAO-TRITON buoy observations at http://www.pmel.noaa.gov/tao/jsdisplay/) and cold biases in model initial subsurface conditions in the equatorial Pacific (Fig. 1, middle panels). Without the Indian Ocean influence, its onset predictions initiated from 1 October 1996 to 1 Mach 1997 basically fail and the predicted peak magnitudes are below 0.5°C (see the green lines in Fig. 2d). Model forecasts from April-May 1997 and later months, however, are not much affected by the Indian Ocean. This probably because the surface and subsurface warming in the eastern Pacific had already become sufficiently strong in April-May 1997 (Figs. 1d and 1j) to initiate unstable air-sea coupled processes in the Pacific for the El Niño growth.

Existing models with a variety of complexities failed to predict the weak-to-moderate 2006-07 El Niño event (McPhaden 2006; see also the real time multi-model ENSO forecasts at http://iri.columbia.edu/climate/ENSO/currentinfo/QuickLook.html), possibly owing to the influences of westerly wind bursts in the western Pacific and intraseasonal oceanic Kelvin waves during the course of its evolution (e.g., Luo 2007; McPhaden 2008). Despite the difficulty, our model correctly predicts the phase transition from La Niña to El Niño in 2006 boreal summer but underestimates its peak magnitude in November-December 2006 (the green and orange lines in Fig. 2e, see also Luo et al. 2007 for our real time forecasts), presumably due to the cold biases in the model initial subsurface conditions (Fig. 1, bottom

panels). Again, suppressing the Indian Ocean influence leads to a long-lasting La Niña throughout 2006 and a complete failure in predicting the El Niño onset (Fig. 2f). This is related to the influence of cold SST anomalies (though small) in the eastern Indian Ocean from the boreal spring to the fall of 2006 in the model predictions (see the green lines in Fig. 6e, possible reasons are discussed below).

Underlying mechanisms for the enhanced El Niño prediction by resolving the Indian Ocean signal can be understood in the following way. Early in the year of El Niño onset, colder than normal SSTs throughout the tropical Indian Ocean sometimes exist as a result of atmospheric response to precedent La Niña in the Pacific (e.g., Klein et al. 1999). This induces anomalous westerlies in the western Pacific, which force an eastward-propagating equatorial downwelling (warm) Kelvin wave along the thermocline in the Pacific (Figs. 3a and 3b) (see also Kug et al. 2005). This tends to terminate the La Niña condition and initiate surface warming in the eastern Pacific which sometimes may trigger unstable air-sea interactions or Bjerknes feedback (Bjerknes 1969) responsible for the El Niño development. The El Niño growth is further enhanced by a subsequent warm Kelvin wave in boreal summer, which is driven by the anomalous westerlies related to the surface cooling and downdraft air over the eastern pole of the growing IOD (Figs. 3a and 3b).

Starting from the middle of the El Niño onset year, well-developed cooling in the eastern Indian Ocean enhances westerly winds in the western-central Pacific (e.g., Saji and Yamagata 2003; Annamalai et al. 2005), thus deepening the central-eastern Pacific thermocline through an eastward-propagating warm Kelvin wave (Figs. 3c and 3d). This

eventually accelerates the growth of El Niño or pseudo-El Niño, particularly in 1994 and 2006 (Fig. 4, see also the orange lines in Fig. 2) when the local Bjerknes feedback in the Pacific is not strong. In the absence of subsurface warming in the east, the major surface warming in the central Pacific associated with the 1994-95 pseudo-El Niño is related to the eastward displacement of warm pool via anomalous surface current advection (Fig. 4a, see also Picaut et al. 1997) driven by the IOD-induced anomalous westerlies in the western Pacific. The anomalous westerlies also tend to weaken the equatorial upwelling and reduce the entrainment of subsurface cold water into the surface layer in the equatorial western and central Pacific (not shown).

In the latter part of the El Niño onset year, contributions from the extreme IOD events to the El Niño growth become generally small (Fig. 2, blue lines). This is not in agreement with previous studies (e.g., Saji and Yamagata 2003; Annamalai et al. 2005) in which they speculated that the peak IOD signal in boreal fall might have large influence on El Niño growth. Contributions of the external forcing to El Niño growth in the latter part of the year appear to be essentially constrained by the intrinsic phase-locking of ENSO to the annual cycle (e.g., Rasmusson and Carpenter 1982). We note that the IOD influence on the El Niño growth in 1997 is much limited after the El Niño onset in boreal summer (see the orange lines in Figs. 2c and 2d, and Fig. 4b). This is probably because the local Bjerknes feedback in the Pacific after the El Niño onset might be already strong enough to support the rapid growth of the 1997-98 El Niño and that the model forecast of the 1997 IOD is less successful (see the orange lines in Fig. 6c, discussed later). The El Niño decay during the following boreal spring, however, appears to be slightly delayed without the Indian Ocean

influence (Fig. 2, blue lines). This is particularly true for the 1998 case, attributed to the simultaneous strong basin-wide surface warming in the Indian Ocean (e.g., Kug et al. 2006).

To further examine the influence of the Indian Ocean on El Niño prediction, we have performed additional forecast experiments of other four El Niño in 1982-83, 1987-88, 1991-92, and 2002-03 with and without the Indian Ocean influence (Fig. 5). In the absence of extreme IOD influence, the prediction differences of the four El Niño between the two experiments appear to be much smaller compared to those of the three El Niño in 1994-95, 1997-98, and 2006-07. The results support the present finding that extreme IOD may have important influence on El Niño development. Without the Indian Ocean influence, a systematic underestimation of the intensity of the 1982-83 El Niño can also be seen (Figs. 5a and 5b, green and orange lines). This is probably related to the impact of an over-predicted IOD in 1982 (see Luo et al. 2007). We note that model prediction of the El Niño onset in 1986 appears to be enhanced by the Indian Ocean basin-wide cooling in late 1985 (not shown); the latter is closely related with the long-lasting La Niña condition in Pacific during late 1983 to early 1986. This is also consistent with the present and existing studies (e.g., Kug et al. 2005, 2006).

b. Influence of ENSO on extreme IOD

Low-level westerly winds blow in the equatorial Indian Ocean throughout most of the year. The winds drive surface eastward currents along the equator, particularly the semi-annual Wyrtki Jets (Wyrtki 1973), pushing the surface water eastward and thereby forming a

deeper thermocline and warm water pool in the east; this is a unique structure compared to the Pacific and Atlantic Oceans (International CLIVAR Project Office 2006). Because of the deep thermocline there, air-sea feedbacks in the Indian Ocean are generally weak compared to ENSO-related air-sea coupling in the Pacific. However, strong Bjerknes feedback may occur during boreal summer when the southeasterly monsoon winds prevail along the west coast of Sumatra and raise the coastal thermocline to be shallow enough, a prerequisite condition for unstable growth of extreme cooling in the eastern Indian Ocean.

Figure 6 shows our model forecasts of the past three extreme IOD events with and without the Pacific influence (see section 2b for the methods). At long-lead times (see the green lines in left panels of Fig. 6), the model shows a limited success in forecasting the extreme IOD, especially in 1994 and 2006.[4] When the Pacific influence is suppressed, surprisingly the model long-lead predictions appear to be improved (see the green lines in right panels of Fig. 6). This is particularly the case for the peak intensities in 1994 and 2006 boreal fall. The model experimental results, however, do not contradict the common notion that ENSO has large influences on the Indian Ocean (e.g., Klein et al. 1999). In fact, the underestimated peak intensity of the extreme IOD in the model retrospective forecasts is primarily caused by a systematic La Niña-like model climate drift in the Pacific (Figs. 7a

[4] Prediction of the 1997 IOD was less successful owing to systematic model biases and bad initial conditions (Luo et al. 2005b and 2007). Besides, the warm intraseasonal event in 1997 boreal spring caused warm subsurface initial conditions, leading to false alarms of a negative IOD for the predictions at mid-lead times (orange lines in Figs. 6c and 6d).

and 8a, see also Luo et al. 2005b and 2008a). This model cold bias, via the atmospheric Walker circulation, induces excessive westerly winds in the Indian Ocean, which hamper the shoaling of thermocline in the east and thereby damp the IOD growth (Figs. 7a and 7b). This suggests the importance of reducing the model climate drift in the Pacific during forecast. Present results also indicate that a part of long-lead predictability of extreme IOD resides in the Indian Ocean itself, in support of our previous studies (Luo et al. 2007 and 2008b). At mid-lead times, the Pacific El Niño influence on the extreme IOD growth appears to be rather limited (orange lines in Fig. 6, and Fig. 7c), indicating a dominant control by the local Bjerknes feedback over the Indian Ocean region.

In summary, our model forecast experiments show that extreme IOD has important influences on El Niño evolution and its onset predictability, and in specific years may induce a different flavor of El Niño (i.e., pseudo-El Niño) with distinctive climate impacts. Besides, the Indo-Pacific inter-basin coupling appears to have substantial impacts on the onset and evolution of both El Niño and extreme IOD via the atmospheric Walker circulation. To further confirm this, we have conducted two "perfect model" prediction experiments by use of a 500-year coupled model simulation (see section 2c for the methods). Totally 25 cases in which extreme IOD co-occurred with El Niño are adopted (Fig. 9). The evolution and spatial patterns of the two climate modes are reproduced realistically in the model.

4. "Perfect model" prediction results

Applicability of the results based on the retrospective forecast experiments (see the previous section) might be limited due to the few co-occurrences of El Niño and extreme IOD in the short observational records. In addition, model biases and errors in initial conditions reduce predictive skill of El Niño and IOD and may lead to unrealistic estimation for the impacts of the inter-basin coupling. In the "perfect model" prediction experiments, errors in both model physics and initial conditions were assumed to be removed. It is worth noting that, although intrinsic model biases might still affect the estimation, some confidence arises from the model's good performance in simulating and predicting the tropical climate (e.g., Yamagata et al. 2004; Luo et al. 2005a,b; Behera et al. 2005 and 2006; Luo et al. 2007 and 2008a,b; Jin et al. 2008).

Apparently, the evolution of both El Niño and extreme IOD cannot be correctly reproduced if the inter-basin coupling is suppressed, particularly during their onset from April to July (gray and green lines in Figs. 10a and 10b). Thus, contributions from the internal air-sea coupled processes in the individual ocean basins are not enough to support their rapid onset and growth. It is worth noting that the internal precursor for the limited long-range predictability of the extreme IOD in the model (gray and green lines in Fig. 10b) comes from the strong anomalous subsurface cooling in the southwestern Indian Ocean (Fig. 11). The cold subsurface anomaly in the southwestern Indian Ocean in boreal winter, that is a response to the cyclonic-like wind forcing in the east about one season ahead (Fig. 11a, see also Xie et al. 2002 and Rao et al. 2002), will propagate westward to the western boundary and then reflect as eastward-propagating equatorial upwelling Kelvin waves in the following seasons (Fig. 11b, see also Rao et al. 2002 and Behera et al. 2006), providing a

long-lead precursor for the extreme IOD evolution. This is consistent with recent observations and model forecast experiments (Horii et al. 2008; Luo et al. 2007 and 2008b).[5]

The underlying physical mechanisms for the inter-basin coupling in the "perfect model" experiments are essentially consistent with those found in the retrospective forecast experiments. Weak basin-wide surface cooling in boreal winter and strong cooling in the eastern Indian Ocean in the following seasons associated with IOD development induce anomalous westerly winds in the western Pacific, which tend to drive two pulses of equatorial warm Kelvin waves in the Pacific during boreal winter and summer, enhancing El Niño onset and growth significantly (Figs. 10c and 10d). SST differences in the equatorial Pacific enhanced by the Indian Ocean signal reach as much as 0.6°-0.8°C in late year (Fig. 10c). In turn, the growing El Niño in the Pacific induces anomalous easterly winds in the Indian Ocean during boreal spring via the atmospheric Walker circulation, raising the thermocline west of Sumatra and thereby reinforcing the onset and growth of IOD significantly (Figs. 10e and 10f). The resemblance of the appearance of these anomaly patterns in the equatorial Indo-Pacific region (compare the middle and bottom panels in Fig.

[5] It is interesting to note that one recent study based on a similar "perfect model" experiment using the GFDL coupled model (Song et al. 2008) found that predictable IOD in that model is largely preconditioned by the tropical Pacific subsurface signal. While the internal subsurface memory in the Indian Ocean plays a little role. Further model inter-comparison study might be helpful to understand the discrepancy.

10) indicates an intrinsic interaction between El Niño and extreme IOD via the Walker circulation. For the predictions initiated after their onsets, the inter-basin coupling also has significant but smaller contributions to their ultimate magnitudes (orange lines in Figs. 10a and 10b, and Fig. 12), in accordance with the retrospective forecast experiment results (Figs. 3 and 7).

5. Summary and discussion

Both El Niño and extreme IOD have large environmental and societal impacts over the globe. Therefore, improving the forecasts of El Niño and extreme IOD, particularly their onsets, has enormous societal benefits. The important influence of ENSO on the Indian Ocean climate (particularly the basin-wide mode) has been well recognized over past decades. However, little has been known for the IOD influence on El Niño and its predictability. Our results based on the retrospective forecast and "perfect model" prediction experiments suggest that extreme IOD has significant contributions to El Niño onset and its long-lead predictability, and hence may have large indirect climate impacts worldwide in addition to its directly related ones. It was found that the IOD also acts to weaken the El Niño-induced drought over India (e.g., Kumar et al. 1999; Ashok et al. 2004). Our results indicate that El Niño and extreme IOD intimately interact with each other via the atmospheric east-west Walker circulation. The Indo-Pacific inter-basin coupling is crucial to the evolution of both El Niño and extreme IOD and their predictions at long-lead times. After their onsets, however, contributions of the inter-basin coupling to their

subsequent growth become limited owing to the dominant role of the local Bjerknes feedback in the individual ocean basins.

In contrast to the pessimism that stresses the role of stochastic forcing in the ENSO predictability (e.g., Flügel et al. 2004), the results presented here provide some optimism: Improving the seasonal forecast of the predictable Indian Ocean climate variability may eventually lead to more skillful El Niño forecasts, and vice versa. The net gain in skill comes from the inter-basin coupling and independent sources for the predictability of the two climate modes. Thus current efforts in establishing a long-term monitoring system in the Indian Ocean (International CLIVAR Project Office 2006) will contribute to better understanding and prediction of not only the Indian Ocean climate but also ENSO in the Pacific. It is surprising that El Niño-like signal can be fully generated by extreme IOD as in 1994, in contrast with classical ENSO theory (see Neelin et al. 1998 for a review). Better understanding of how El Niño and IOD might evolve and influence each other under global warming may have important implications for the future projection of the climate on Earth. Noticing the more frequent occurrences of extreme IOD and pseudo-El Niño in recent decades (e.g., Trenberth and Stepaniak 2001; Ashok et al. 2007), probably in association with the weakened Walker circulation in response to anthropogenic forcing (Vecchi et al. 2006) and decadal El Niño-like variability in the Pacific (e.g., Luo and Yamagata 2001), it is conceivable that the intensified IOD activity (Ihara et al. 2008; Abram et al. 2008) would play a more important role in El Niño evolution under the present global warming trend. This may have implications for our future projection of ENSO under the global warming.

Acknowledgements. Satellite SST observations were provided by NOAA/OAR/ESRL, available at http://www.cdc.noaa.gov/cdc/data.noaa.oisst.v2.html. All model experiments were carried out on the JAMSTEC Earth Simulator. We thank S.-P. Xie for helpful discussions, and two anonymous reviewers for their valuable comments that helped to improve the manuscript.

References

Abram, N. J., M. K. Gagan, J. E. Cole, W. S. Hantoro, and M. Mudelsee, 2008: Recent intensification of tropical climate variability in the Indian Ocean. *Nature Geoscience* **1,** 849-853.

Annamalai, H., S.-P. Xie, J. P. McCreary, and R. Murtugudde, 2005: Impact of Indian Ocean sea surface temperature on developing El Niño. *J. Climate*, **18,** 302-319.

Ashok, K., Z. Guan, N. H. Saji, and T. Yamagata, 2004: Individual and combined influences of ENSO and the Indian Ocean Dipole on the Indian summer monsoon. *J. Climate*, **17,** 3141-3155.

Ashok, K., S. K. Behera, S. A. Rao, H. Weng, and T. Yamagata 2007: El Niño Modoki and its possible teleconnection. *J. Geophys. Res.*, **112,** C11007, doi:10.1029/2006JC003798.

Barnston, A. G., M. H. Glantz, and Y. He, 1999: Predictive skill of statistical and dynamical climate models in SST forecasts during the 1997-98 El Niño episode and the 1998 La Niña onset. *Bull. Amer. Meteor. Soc.*, **80,** 217–243.

Behera, S. K., J.-J. Luo, S. Masson, P. Delecluse, S. Gualdi, A. Navarra, and T. Yamagata, 2005: Paramount impact of the Indian Ocean Dipole on the East African short rain: A CGCM study. *J. Climate*, **18,** 4514–4530.

Behera, S. K., J.-J. Luo, S. Masson, S. A. Rao, H. Sakuma, and T. Yamagata, 2006: A CGCM study on the interaction between IOD and ENSO. *J. Climate*, **19,** 1688-1705.

Bjerknes, J., 1969: Atmospheric teleconnections from the equatorial Pacific. *Mon. Wea. Rev.*, **97,** 163-172.

Chang, P., and S. G. Philander, 1994: A coupled ocean-atmosphere instability of relevance to the seasonal cycle. *J. Atmos. Sci.*, **51,** 3627-3648.

Chen, D., M. A. Cane, A. Kaplan, S. E. Zebiak, and D. Huang, 2004: Predictability of El Niño over the past 148 years. *Nature*, **428,** 733–736.

Fedorov, A. V., S. L. Harper, S. G. Philander, B. Winter, and A. Wittenberg, 2003: How predictable is El Niño? *Bull. Amer. Meteor. Soc.*, **84**, 911–919.

Flügel, M., P. Chang, and C. Penland, 2004: The role of stochastic forcing in modulating ENSO predictability. *J. Climate*, **17,** 3125–3140.

Gebbie, G., I. Eisenman, A. Wittenberg, and E. Tziperman, 2007: Modulation of westerly wind bursts by sea surface temperature: A semistochastic feedback for ENSO. *J. Atmos. Sci.*, **64,** 3281-3295.

Gualdi, S., A. Navarra, E. Guilyardi, and P. Delecluse, 2003: Assessment of the tropical Indo-Pacific climate in the SINTEX CGCM. *Ann. of Geophys.*, **46,** 1-26.

Guilyardi, E., P. Delecluse, S. Gualdi, and A. Navarra, 2003: Mechanisms for ENSO phase change in a coupled GCM. *J. Climate*, **16,** 1141-1158.

Hong, C.-C., T. Li, L. Ho, and J.-S. Kug, 2008a: Asymmetry of the Indian Ocean Dipole. Part I: Observational analysis. *J. Climate*, **21,** 4834-4848.

Hong, C.-C., T. Li, and J.-J. Luo, 2008b: Asymmetry of the Indian Ocean Dipole. Part II: Model diagnosis. *J. Climate*, **21,** 4849-4858.

Horel, J. D., 1982: On the annual cycle of the tropical Pacific atmosphere and ocean. *Mon. Wea. Rev.*, **110,** 1863-1877.

Horii, T., H. Hase, I. Ueki, and Y. Masumoto, 2008: Oceanic precondition and evolution of the 2006 Indian Ocean dipole. *Geophys. Res. Lett.*, **35,** L03607 10.1029/2007GL032464.

Ihara, C., Y. Kushnir, and M. A. Cane, 2008: Warming trend of the Indian Ocean SST and Indian Ocean Dipole from 1880 to 2004. *J. Climate*, **21,** 2035-2046.

International CLIVAR Project Office, 2006: Understanding the role of the Indian Ocean in the climate system-Implementation plan for sustained observations. *CLIVAR Publ. Ser.* **100,** 76 pp., available at http://eprints.soton.ac.uk/20357/.

Jin, E. K., and Coauthors, 2008: Current status of ENSO prediction skill in coupled ocean–atmosphere models. *Climate Dyn.*, **31,** 647-664.

Jin, F.-F., 1997: An equatorial ocean recharge paradigm for ENSO. Part I: Conceptual model. *J. Atmos. Sci.*, **54,** 811–829.

Kessler, W. S., 2002: Is ENSO a cycle or a series of events? *Geophys. Res. Lett.*, **29,** 2125, doi:10.1029/2002GL015924.

Klein, S. A., B. J. Soden, and N.-C. Lau, 1999: Remote sea surface temperature variations during ENSO: Evidence for a tropical atmospheric bridge. *J. Climate*, **12,** 917-932.

Kug, J.-S., S.-I1 An, F.-F. Jin, and I.-S. Kang, 2005: Preconditions for El Niño and La Niña onsets and their relation to the Indian Ocean. *Geophys. Res. Lett.*, **32,** L05706, doi:10.1029/2004GL021674.

Kug, J.-S., T. Li, S.-I. An, I.-S. Kang, J.-J. Luo, S. Masson, and T. Yamagata, 2006: Role of the ENSO–Indian Ocean coupling on ENSO variability in a coupled GCM. *Geophys. Res. Lett.*, **33,** L09710, doi:10.1029/2005GL024916.

Kumar, K. K., B. Rajagopalan, and M. A. Cane, 1999: On the weakening relationship

between the Indian Monsoon and ENSO. *Science*. **284,** 2156–2159.

Kumar, K. K., B. Rajagopalan, M. Hoerling, G. Bates, and M. Cane, 2006: Unraveling the mystery of Indian monsoon failure during El Niño events. *Science*, **314,** 115–119.

Landsea, C. W., and J. A. Knaff, 2000: How much skill was there in forecasting the very strong 1997/98 El Niño? *Bull. Amer. Meteor. Soc.*, **81**, 2107–2119.

Luo, J.-J., and T. Yamagata, 2001: Long-term El Niño-Southern Oscillation (ENSO)-like variation with special emphasis on the South Pacific. *J. Geophys. Res.*, **106**, 22211–22227.

Luo, J.-J., S. Masson, S. Behera, P. Delecluse, S. Gualdi, A. Navarra, and T. Yamagata, 2003: South Pacific origin of the decadal ENSO-like variation as simulated by a coupled GCM. *Geophys. Res. Lett.,* **30**, 2250, doi:10.1029/2003GL018649.

Luo, J.-J., S. Masson, E. Roeckner, G. Madec, and T. Yamagata, 2005a: Reducing climatology bias in an ocean-atmosphere CGCM with improved coupling physics. *J. Climate*, **18,** 2344–2360.

Luo, J.-J., S. Masson, S. Behera, S. Shingu, and T. Yamagata, 2005b: Seasonal climate predictability in a coupled OAGCM using a different approach for ensemble forecasts. *J. Climate*, **18,** 4474–4497.

Luo, J.-J., 2007: Predicting the weak El Niño in 2006/07 winter and La Niña condition in 2007. *APCC Newsletter*, **2**(1), 5-7 (available at http://www.apcc21.net).

Luo, J.-J. , S. Masson, S. Behera, and T. Yamagata, 2007: Experimental forecasts of the Indian Ocean Dipole using a coupled OAGCM. *J. Climate*, **20,** 2178-2190.

Luo, J.-J., S. Masson, S. Behera, and T. Yamagata, 2008a: Extended ENSO predictions using a fully coupled ocean–atmosphere model. *J. Climate*, **21,** 84-93.

Luo, J.-J., S. Behera, Y. Masumoto, H. Sakuma, and T. Yamagata, 2008b: Successful prediction of the consecutive IOD in 2006 and 2007. *Geophys. Res. Lett.*, **35,** L14S02, doi:10.1029/2007GL032793.

Madec, G., P. Delecluse, M. Imbard, and C. Levy, 1998: OPA 8.1 ocean general circulation model reference manual. LODYC/IPSL Tech. Rep. Note 11, Paris, France, 91 pp.

Masson, S., and Coauthors, 2005: Impact of barrier layer on winter-spring variability of the southeastern Arabian Sea, *Geophys. Res. Lett*. **32,** L07703, doi:10.1029/2004GL021980.

McPhaden, M. J., 1999: Genesis and evolution of the 1997-98 El Niño. *Science*, **283,** 950–954.

McPhaden, M. J., 2006: ENSO as an integrating concept in Earth Science. *Science*, **314,** 1740-1745.

McPhaden, M. J., X. Zhang, H. H. Hendon, and M. C. Wheeler, 2006: Large scale dynamics and MJO forcing of ENSO variability. *Geophys. Res. Lett*., **33,** L16702, doi:10.1029/2006GL026786.

McPhaden, M. J., 2008: Evolution of the 2006–2007 El Niño: the role of intraseasonal to interannual time scale dynamics. *Adv. Geosci.*, **14**, 219–230.

Meyers, G., 1996: Variations of Indonesia Throughflow and the El Niño-Southern Oscillation. *J. Geophys. Res.*, **101,** 12255-12263.

Meyers, G., P. McIntosh, L. Pigot, and M. Pook, 2007: The years of El Niño, La Niña, and interactions with the tropical Indian Ocean. *J. Climate*, **20,** 2872-2880.

Neelin, J. D., D. S. Battisti, A. C. Hirst, F.-F. Jin, Y. Wakata, T. Yamagata, and S. Zebiak, 1998: ENSO theory. *J. Geophys. Res.,* **103,** 14261–14290.

Palmer, T. N., and Coauthors, 2004: Development of a European multimodel ensemble system for seasonal-to-interannual prediction (DEMETER). *Bull. Amer. Meteor. Soc.*, **85,** 853–872.

Picaut, J., F. Masia, and Y. du Penhoat, 1997: An advective-reflective conceptual model for the oscillatory nature of the ENSO. *Science*, **277,** 663-666.

Rao, S. A., S. Behera, Y. Masumoto, and T. Yamagata, 2002: Interannual variability in the subsurface Indian Ocean with special emphasis on the Indian Ocean Dipole. *Deep Sea Res.*, **49,** 1549-1572.

Rasmusson, E. M., and T. H. Carpenter, 1982: Variations in tropical sea surface temperature and surface wind fields associated with the Southern Oscillation/El Niño. *Mon. Wea. Rev.*, **110,** 354-384.

Reynolds, R. W., N. A. Rayner, T. M. Smith, D. C. Stokes, and W. Wang, 2002: An improved in situ and satellite SST analysis for climate. *J. Climate*, **15,** 1609–1625.

Roeckner, E., and Coauthors, 1996: The atmospheric general circulation model ECHAM-4: Model description and simulation of present-day climate. Max-Planck-Institut für Meteorologie Rep. 218, Hamburg, Germany, 90 pp.

Saji, N. H., B. N. Goswami, P. N. Vinayachandran, and T. Yamagata, 1999: A dipole mode in the tropical Indian Ocean. *Nature*, **401,** 360-363.

Saji, N. H., and T. Yamagata, 2003: Structure of SST and surface wind variability during Indian Ocean Dipole model events: COADS observations. *J. Climate*, **16,** 2735-2751.

Sara, S., and Coauthors, 2006: The NCEP climate forecast system. *J. Climate*, **19,** 3483-3517.

Song, Q., G. A. Vecchi, and A. J. Rosati, 2008: Predictability of the Indian Ocean sea surface temperature anomalies in the GFDL coupled model. *Geophys. Res. Let.*, **35,** L02701, 273 doi:10.1029/2007GL031966.

Trenberth, K. E., and D. P. Stepaniak, 2001: Indices of El Niño evolution, *J. Climate*, **14,** 1697-1701.

Valcke, S., L. Terray, and A. Piacentini, 2000: The OASIS coupler user guide version 2.4. CERFACE Tech. Rep. TR/CGMC/00-10, 85 pp.

Vecchi, G. A., B. J. Soden, A. T. Wittenberg, I. M. Held, A. Leetmaa, and M. J. Harrison, 2006: Weaking of tropical Pacific atmospheric circulation due to anthropogenic forcing. *Nature*, **441,** 73-76.

Wang, G., and H. H. Hendon, 2007: Sensitivity of Australian rainfall to inter-El Niño variations. *J. Climate*, **20,** 4211-4226.

Webster, P. J., A. Moore, J. Loschnigg, and M. Leban, 1999: Coupled ocean–atmosphere dynamics in the Indian Ocean during 1997–98. *Nature*, **401,** 356-360.

Weng, H., K. Ashok, S. K. Behera, S. A. Rao, and T. Yamagata, 2007: Impacts of recent El Niño Modoki on dry/wet conditions in the Pacific rim during boreal summer. *Climate Dyn.*, **29,** 113-129.

Wu, R., and B. P. Kirtman, 2004: Understanding the impacts of the Indian Ocean on ENSO variability in a coupled GCM. *J. Climate*, **17,** 4019-4031.

Wyrtki, K., 1973: An equatorial jet in the Indian Ocean. *Science*, **181,** 262-264.

Xie, S.-P., H. Annamalai, F. A. Schott, and J. P. McCreary, 2002: Origin and predictability of South Indian Ocean climate variability. *J. Climate*, **15,** 864-874.

Yamagata, T., S. Behera, J.-J. Luo, S. Masson, M. Jury, and S. A. Rao, 2004: Coupled ocean-atmosphere variability in the tropical Indian Ocean. Earth's Climate: *The Ocean-Atmosphere Interaction. Geophys. Monogr.* **147,** Amer. Geophys. Union, 189-212.

Yu, J.-Y., C. R. Mechoso, J. C. McWilliams, and A. Arakawa, 2002: Impacts of the Indian Ocean on the ENSO cycle. *Geophys. Res. Lett.*, **29,** 1204 10.1029/2001GL014098.

Figure Captions:

Figure 1: Upper-ocean temperature anomalies (°C, relative to the 1983-2006 climatology) along the equatorial (2°S-2°N) Pacific. (a) Model results during October-December 1993 (colored scale) and January-March 1994 (contours). Contour interval is 0.5°C; thick solid lines indicate zero contour. (b) As in (a), but for those during April-June 1994 (colored scale) and July-September 1994 (contours). (c-d) and (e-f) As in (a-b), but for the temperature anomalies associated with the 1997-98 and 2006-07 El Niño evolutions. These are model 9-member ensemble mean initial conditions for forecasts, produced by the coupled SST-nudging initialization approach (see Luo et al. 2005b and 2007). (g-l) As in (a-f), but for the results from National Centers for Environmental Prediction (NCEP) ocean reanalysis, available at http://www.cpc.ncep.noaa.gov/products/GODAS/. Subsurface temperature anomalies in the equatorial Indian Ocean were not shown for comparison because of sparse observations there.

Figure 2: SST anomalies in the Niño3.4 region (5°S-5°N, 120°-170°W) of the three El Niño events in 1994-95, 1997-98, and 2006-07. The black curves are satellite observations and colored curves 9-member ensemble mean forecasts for 12 target months. Three gray lines indicate the forecasts initiated from 1 July, 1 August, and 1 September of the year before the El Niño, six green lines are the predictions starting from the next 6 consecutive months, and so forth for the six orange and three blue lines. Left panels show the model forecasts with active air-sea coupling in all oceans (hereafter referred to as CTL), and right

panels the results without the tropical Indian Ocean climate variability (dIO). The long-dashed lines indicate the criterion (0.5°C) for the El Niño onset. The ensemble forecast anomaly was calculated relative to the model climatology of 1983-2006, thereby removing the model climate drifts *a posteriori*. To clearly show the differences, the same model climatology produced in the CTL experiment was used to calculate the forecast anomaly for the dIO experiment.

Figure 3: (a) SST (°C, colored scale), zonal wind at 10 m height (U10, solid/dashed contours indicate positive/negative values. Contour interval: ±0.5, ±1, ±1.5 m/s, ...) and (b) 20°C isotherm depth (D20, in meters, representing the depth of the equatorial thermocline) difference along the equator (2°S-2°N) between the CTL and dIO retrospective forecast experiments starting from 1 January of YR(0) (i.e., El Niño and IOD developing year). (c-d) As in (a-b), but for differences of the forecasts from 1 June of YR(0). These results, produced by the average of three cases (i.e., 1994, 1997 and 2006), indicate the effects of the Indian Ocean on El Niño growth.

Figure 4: IOD influence on El Niño prediction. (a) SST (colored scale) and upper 50 m ocean zonal current (U50m, contour interval of 5 cm/s with zero contour omitted) difference during November 1994 to January 1995 between the CTL and dIO retrospective forecast experiments starting from 1 June 1994. (b-c) As in (a), but for those associated with the 1997-98 and 2006-07 El Niño.

Figure 5: Same as in Fig. 2, but for model forecasts of other four El Niño events in 1982-83, 1987-88, 1991-92, and 2002-03 with and without the Indian Ocean influence.

Figure 6: Same as in Fig. 2, but for model forecasts of the SST anomaly in the eastern Indian Ocean (EIO, 10°S-0°, 90°-110°E). Unstable growth of strong surface cooling in this region was found to be closely related to the Bjerknes feedback associated with strong coastal upwelling (Saji et al. 1999; Meyers et al. 2007), which plays a key role in initiating the extreme IOD evolution. Left panels show the model forecasts in the CTL experiment, and right panels the results without the Pacific Ocean climate variations (dPO).

Figure 7: Same as in Fig. 3, but for the differences between the CTL and dPO forecast experiments. The results indicate the effects of the Pacific signals on the extreme IOD development.

Figure 8: Same as in Fig. 7, but for the model climate drift of the CTL retrospective forecasts based on the climatology of 1983-2006. The climate drift refers to the deviation of the model climatology (a function of start month and lead time) from the observations. The "observed" U10 and D20 used here were produced in the model based on the coupled SST-nudging initialization approach (see Luo et al. 2005b and 2007). The westward-propagating cold SST drift in the Pacific (left panels) is not related to model thermocline drift (right panels); this is reminiscent of the physical processes responsible for the westward-propagating annual cycle of SST (e.g., Horel 1982; Chang and Philander 1994).

Figure 9: Co-occurred El Niño and extreme IOD in the model. (a) Niño3.4 (solid lines) and EIO (dashed lines) SST anomaly from satellite observations (3 cases, red lines) and free coupled model simulations (25 cases, green lines). Thick curves indicate the averaged values. (b-c) Model and observed SST anomalies during September-November of YR(0) in the tropical Indo-Pacific region. The observed (model) anomaly is relative to the climatology of 1983-2006 (500-year simulations).

Figure 10: Inter-influence between El Niño and extreme IOD in the "perfect model" prediction experiments. (a) Niño3.4 and (b) EIO SST anomaly produced in the free coupled model simulation (CTL, black lines) and "perfect model" prediction experiments without the air-sea coupling in the individual basins separately (colored lines). The anomaly was calculated relative to the model 500-year mean climatology and averaged for the 25 cases in which El Niño and extreme IOD co-occurred. (c-d) Same as in Figs. 3a and 3b, but for the results based on the "perfect model" prediction experiments. Solid (dashed) light-gray lines indicate a 95% (90%) confidence level for the SST and D20 differences based on two-tail Student's t-test in the Pacific (i.e., the influence from the Indian Ocean) and one-tail t-test in the Indian Ocean (i.e., the composite anomaly of the 25 extreme IOD events), respectively. (e-f**)** As in (c-d), but for the El Niño influence on the extreme IOD prediction.

Figure 11: (a) Composite anomalies of model D20 during December of YR(-1) to February of YR(0) and surface winds during September-November of YR(-1) in the tropical Indian

Ocean prior to the occurrences of the 25 extreme IOD. (b) D20 and U10 (contour interval: ±0.5, ±1, ±1.5 m/s, ...) anomaly along the equator.

Figure 12: (a-d) Same as in Figs. 10c-f, but for the "perfect model" prediction experiments starting from 1 June of YR(0). The reduced feedback between El Niño and extreme IOD after their onsets (compared to Figs. 10c-f, see also Figs. 3 and 7) suggests the dominant role of the local Bjerknes feedback in the individual basins during the subsequent growth of these two climate modes, each of which is also subject to their intrinsic annual-phase locking (e.g., Rasmusson and Carpenter 1982; Saji et al. 1999).

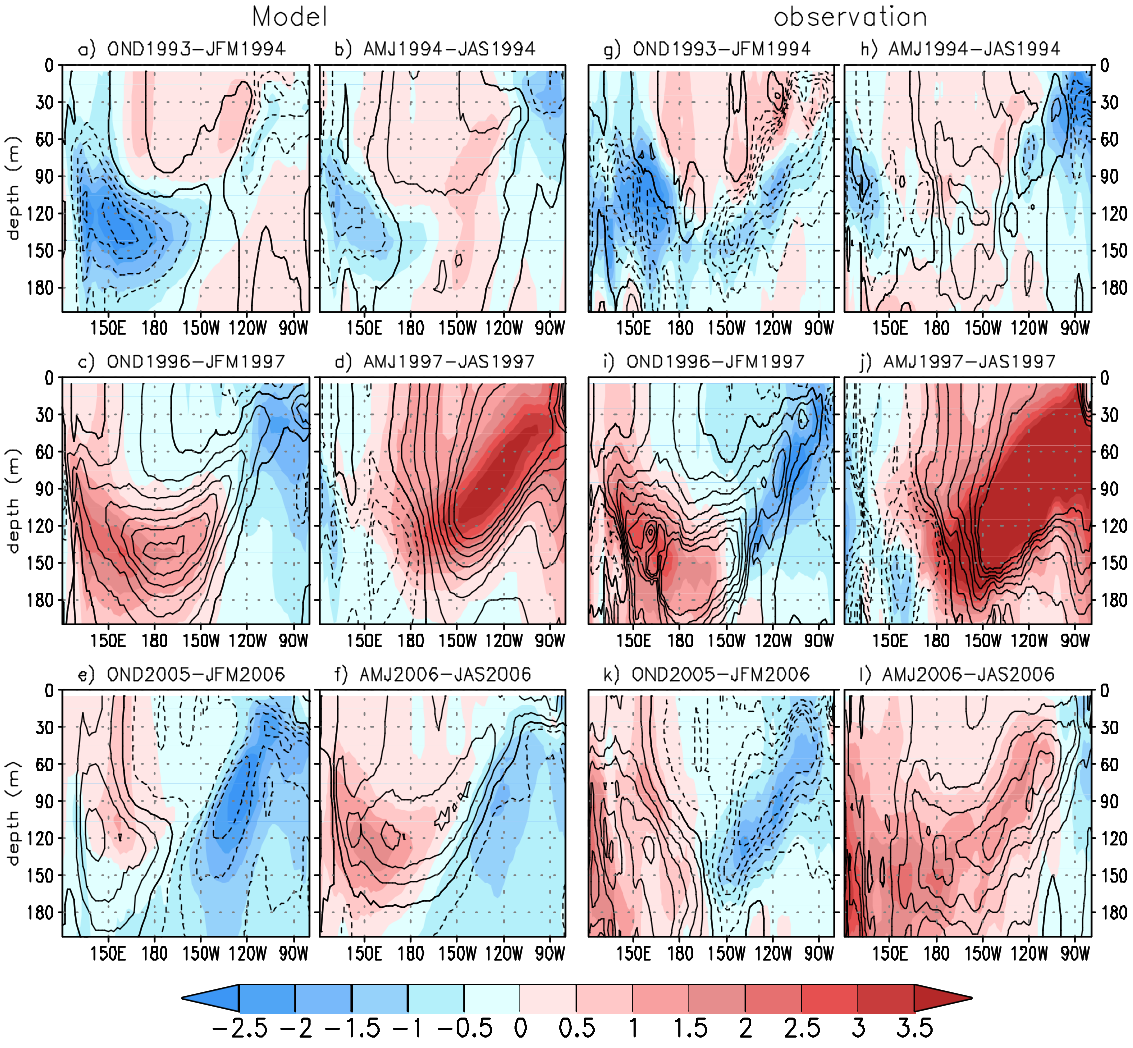

Figure 1: Upper-ocean temperature anomalies (°C, relative to the 1983-2006 climatology) along the equatorial (2°S-2°N) Pacific. (a) Model results during October-December 1993 (colored scale) and January-March 1994 (contours). Contour interval is 0.5°C; thick solid lines indicate zero contour. (b) As in (a), but for those during April-June 1994 (colored scale) and July-September 1994 (contours). (c-d) and (e-f) As in (a-b), but for the temperature anomalies associated with the 1997-98 and 2006-07 El Niño evolutions. These are model 9-member ensemble mean initial conditions for forecasts, produced by the coupled SST-nudging initialization approach (see Luo et al. 2005b and 2007). (g-l) As in (a-f), but for the results from National Centers for Environmental Prediction (NCEP) ocean reanalysis, available at http://www.cpc.ncep.noaa.gov/products/GODAS/. Subsurface temperature anomalies in the equatorial Indian Ocean were not shown for comparison because of sparse observations there.

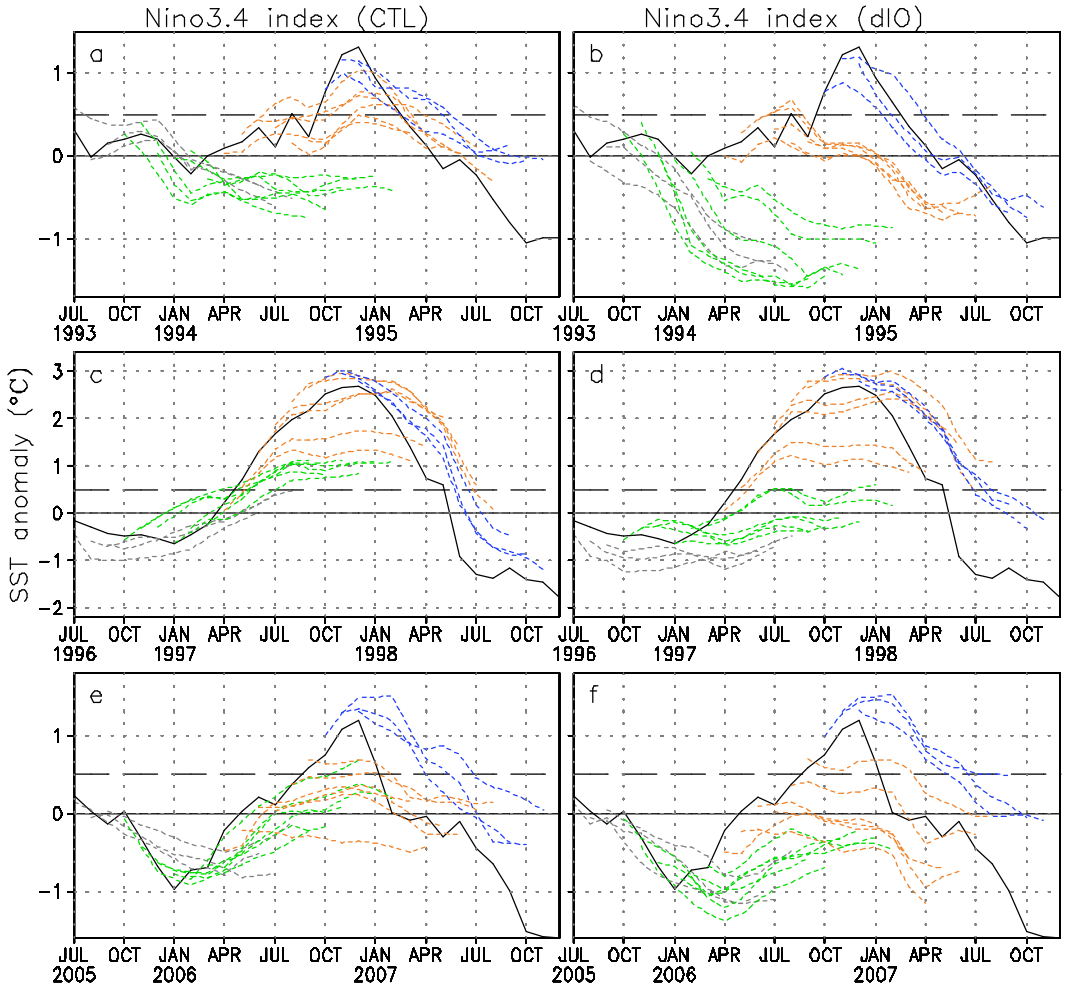

Figure 2: SST anomalies in the Niño3.4 region (5°S-5°N, 120°-170°W) of the three El Niño events in 1994-95, 1997-98, and 2006-07. The black curves are satellite observations and colored curves 9-member ensemble mean forecasts for 12 target months. Three gray lines indicate the forecasts initiated from 1 July, 1 August, and 1 September of the year before the El Niño, six green lines are the predictions starting from the next 6 consecutive months, and so forth for the six orange and three blue lines. Left panels show the model forecasts with active air-sea coupling in all oceans (hereafter referred to as CTL), and right panels the results without the tropical Indian Ocean climate variability (dIO). The long-dashed lines indicate the criterion (0.5°C) for the El Niño onset. The ensemble forecast anomaly was calculated relative to the model climatology of 1983-2006, thereby removing the model climate drifts *a posteriori*. To clearly show the differences, the same model climatology produced in the CTL experiment was used to calculate the forecast anomaly for the dIO experiment.

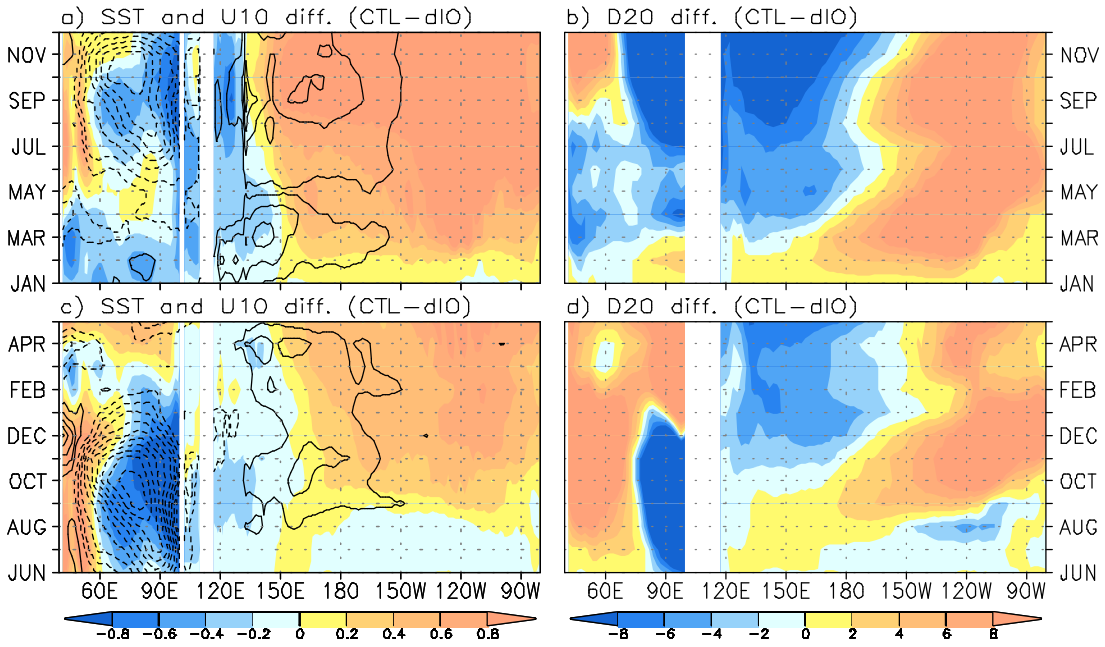

Figure 3: (a) SST (°C, colored scale), zonal wind at 10 m height (U10, solid/dashed contours indicate positive/negative values. Contour interval: ±0.5, ±1, ±1.5 m/s, ...) and (b) 20°C isotherm depth (D20, in meters, representing the depth of the equatorial thermocline) difference along the equator (2°S-2°N) between the CTL and dIO retrospective forecast experiments starting from 1 January of YR(0) (i.e., El Niño and IOD developing year). (c-d) As in (a-b), but for differences of the forecasts from 1 June of YR(0). These results, produced by the average of three cases (i.e., 1994, 1997 and 2006), indicate the effects of the Indian Ocean on El Niño growth.

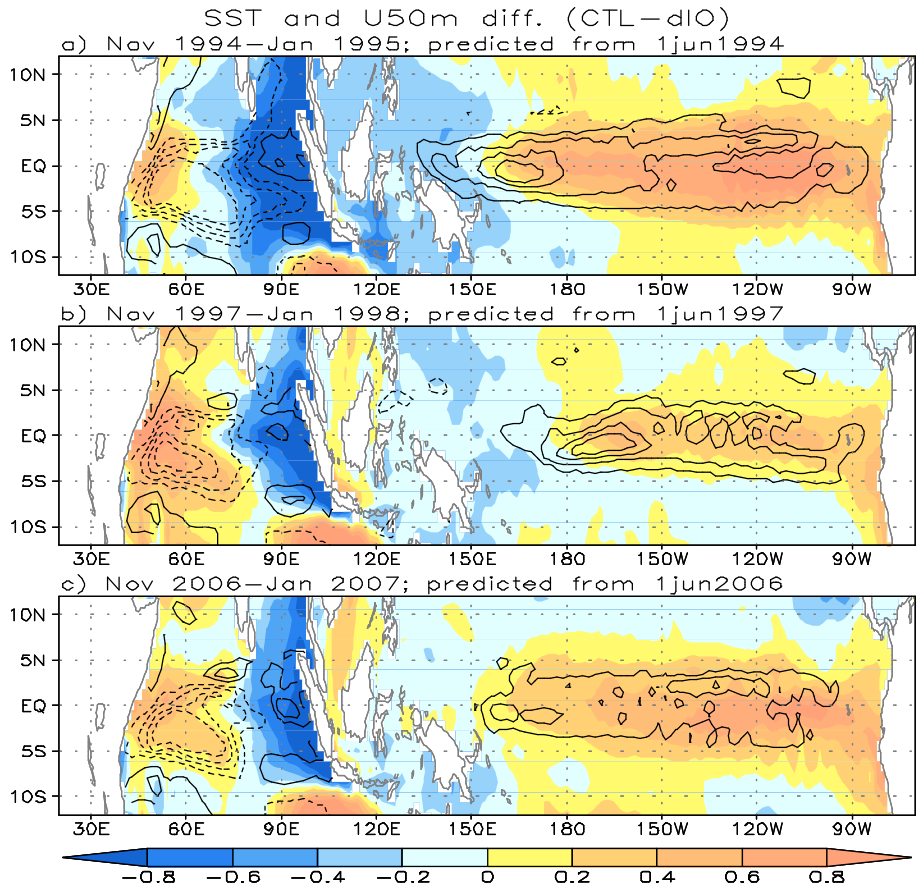

Figure 4: IOD influence on El Niño prediction. (a) SST (colored scale) and upper 50 m ocean zonal current (U50m, contour interval of 5 cm/s with zero contour omitted) difference during November 1994 to January 1995 between the CTL and dIO retrospective forecast experiments starting from 1 June 1994. (b-c) As in (a), but for those associated with the 1997-98 and 2006-07 El Niño.

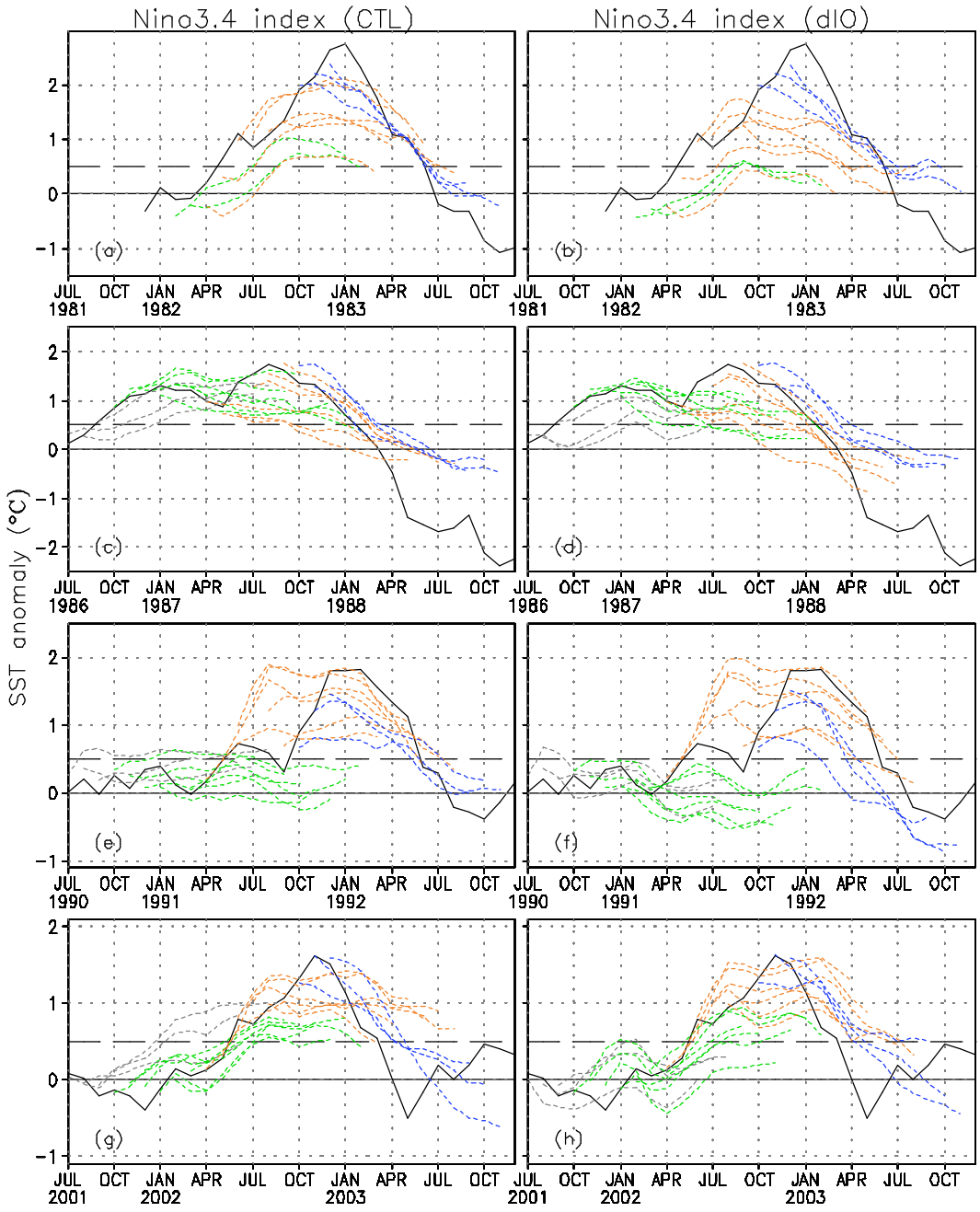

Figure 5: Same as in Fig. 2, but for model forecasts of other four El Niño events in 1982-83, 1987-88, 1991-92, and 2002-03 with and without the Indian Ocean influence.

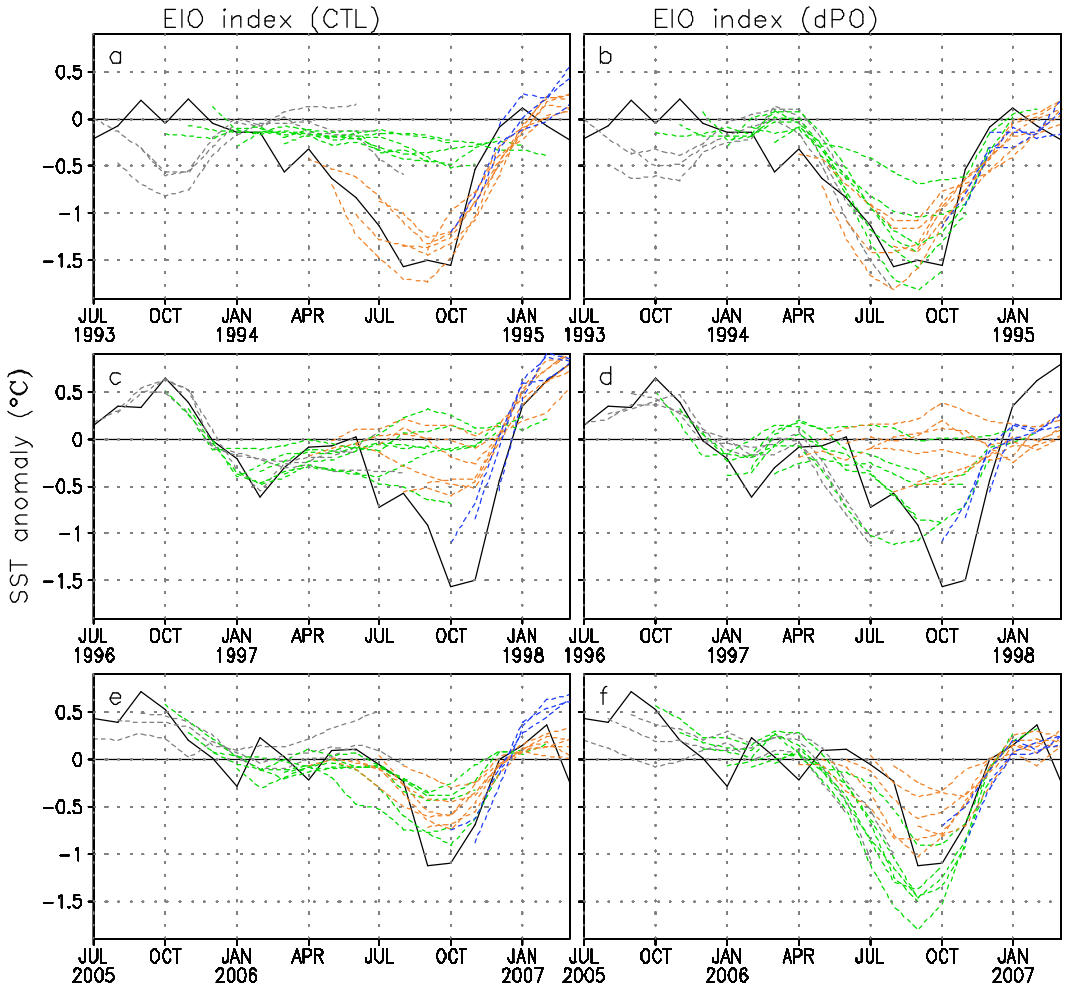

Figure 6: Same as in Fig. 2, but for model forecasts of the SST anomaly in the eastern Indian Ocean (EIO, 10°S-0°, 90°-110°E). Unstable growth of strong surface cooling in this region was found to be closely related to the Bjerknes feedback associated with strong coastal upwelling (Saji et al. 1999; Meyers et al. 2007), which plays a key role in initiating the extreme IOD evolution. Left panels show the model forecasts in the CTL experiment, and right panels the results without the Pacific Ocean climate variations (dPO).

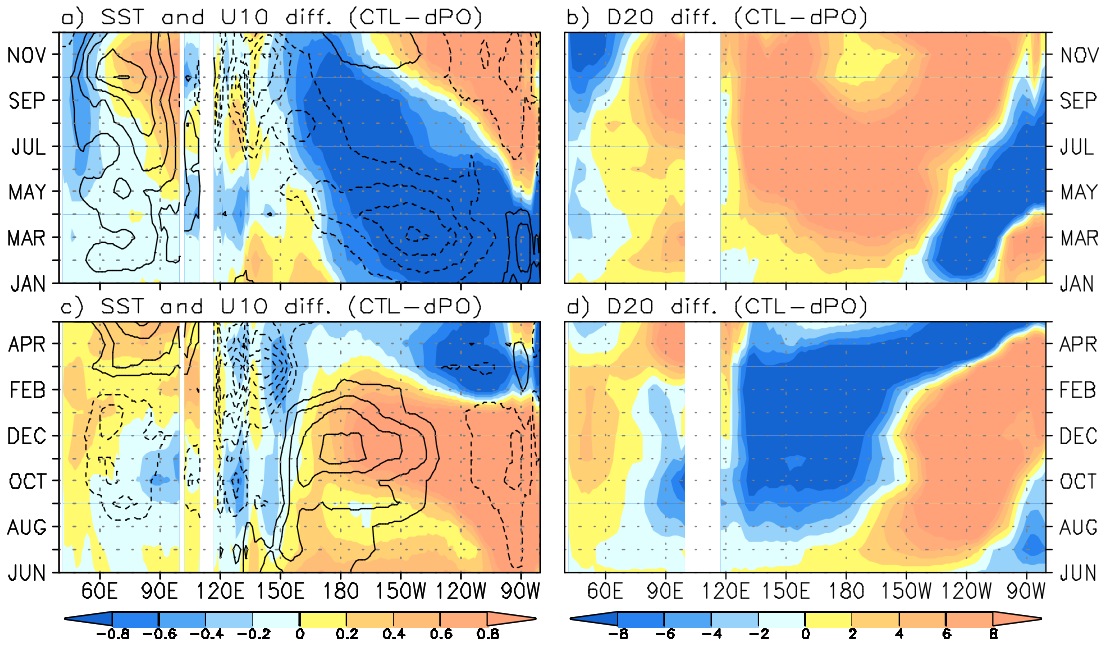

Figure 7: Same as in Fig. 3, but for the differences between the CTL and dPO forecast experiments. The results indicate the effects of the Pacific signals on the extreme IOD development.

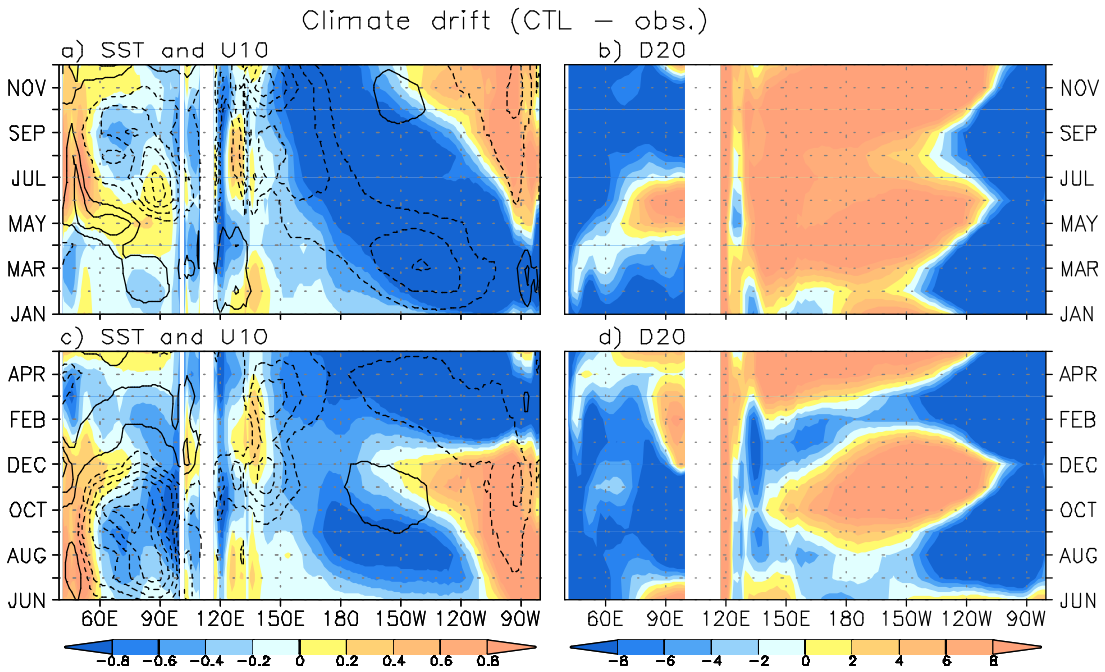

Figure 8: As in Fig. 7, but for the model climate drift of the CTL retrospective forecasts based on the climatology of 1983-2006. The climate drift refers to the deviation of the model climatology (a function of start month and lead time) from the observations. The "observed" U10 and D20 used here were produced in the model based on the coupled SST-nudging initialization approach (see Luo et al. 2005b and 2007). The westward-propagating cold SST drift in the Pacific (left panels) is not related to model thermocline drift (right panels); this is reminiscent of the physical processes responsible for the westward-propagating annual cycle of SST (e.g., Horel 1982; Chang and Philander 1994).

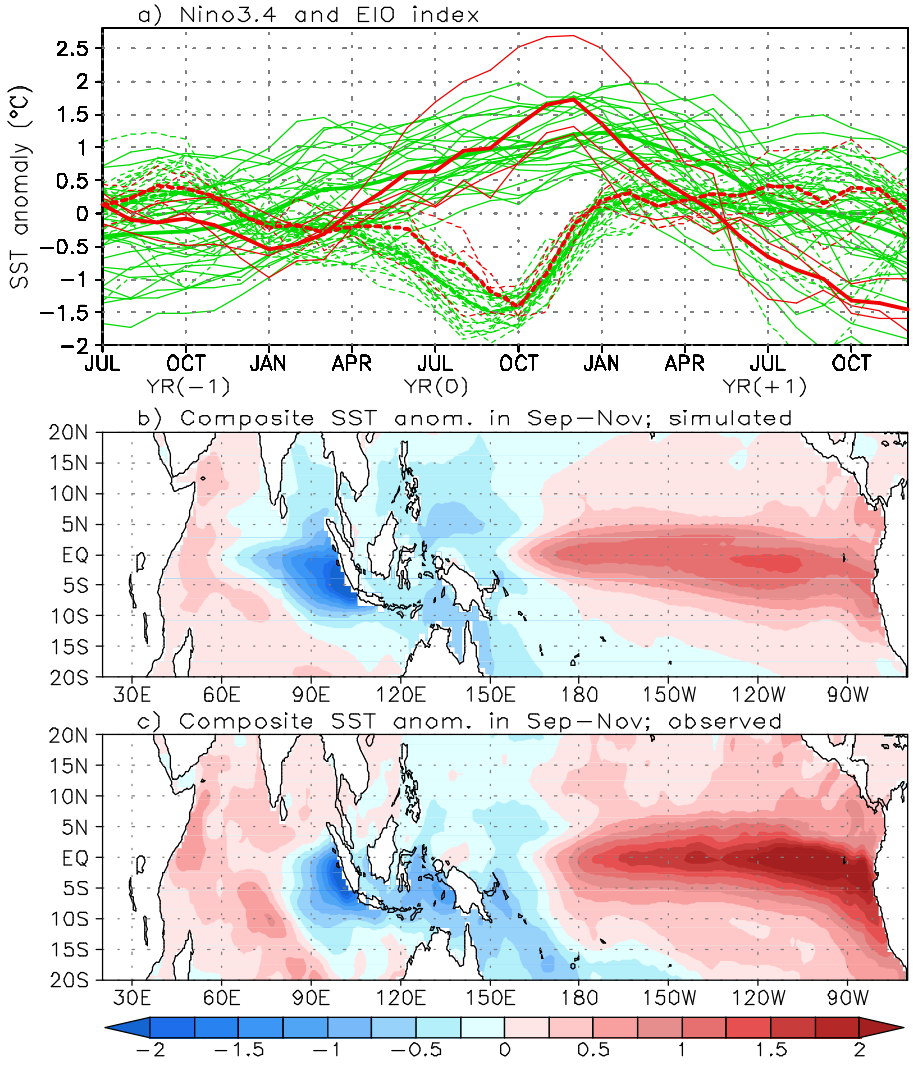

Figure 9: Co-occurred El Niño and extreme IOD in the model. (a) Niño3.4 (solid lines) and EIO (dashed lines) SST anomaly from satellite observations (3 cases, red lines) and free coupled model simulations (25 cases, green lines). Thick curves indicate the averaged values. (b-c) Model and observed SST anomalies during September-November of YR(0) in the tropical Indo-Pacific region. The observed (model) anomaly is relative to the climatology of 1983-2006 (500-year simulations).

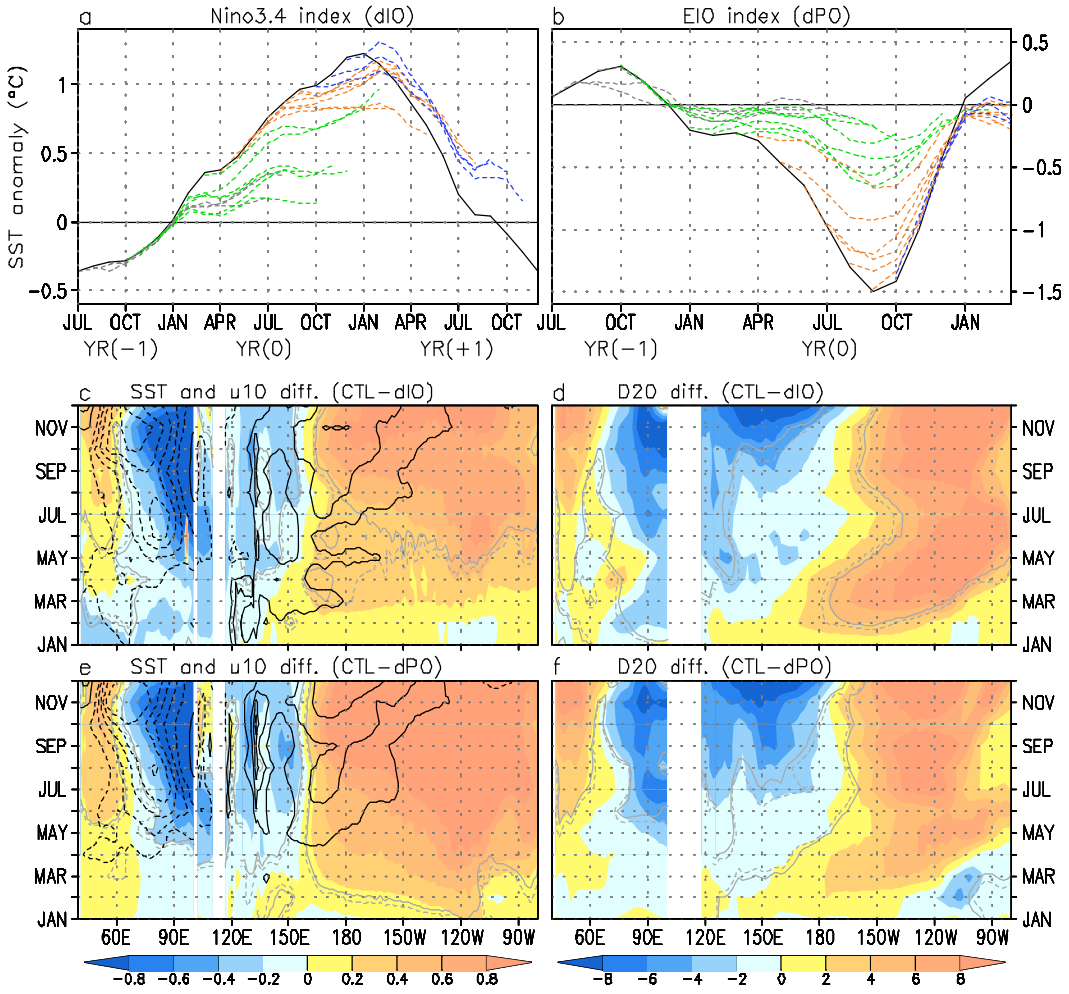

Figure 10: Inter-influence between El Niño and extreme IOD in the "perfect model" prediction experiments. (a) Niño3.4 and (b) EIO SST anomaly produced in the free coupled model simulation (CTL, black lines) and "perfect model" prediction experiments without the air-sea coupling in the individual basins separately (colored lines). The anomaly was calculated relative to the model 500-year mean climatology and averaged for the 25 cases in which El Niño and extreme IOD co-occurred. (c-d) Same as in Figs. 3a and 3b, but for the results based on the "perfect model" prediction experiments. Solid (dashed) light-gray lines indicate a 95% (90%) confidence level for the SST and D20 differences based on two-tail Student's t-test in the Pacific (i.e., the influence from the Indian Ocean) and one-tail t-test in the Indian Ocean (i.e., the composite anomaly of the 25 extreme IOD events), respectively. (e-f**)** As in (c-d), but for the El Niño influence on the extreme IOD prediction.

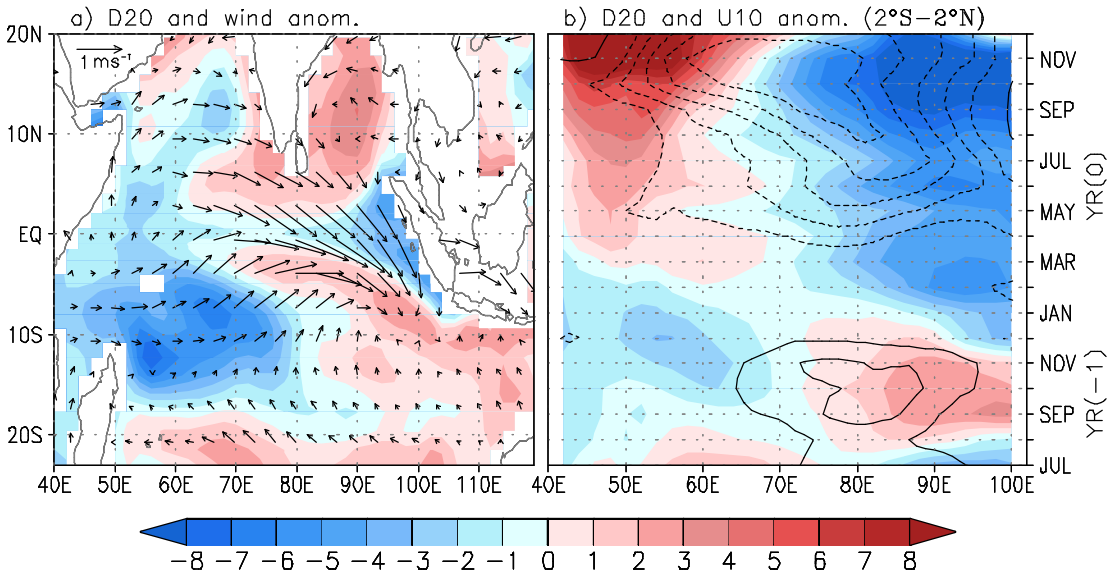

Figure 11: (a) Composite anomalies of model D20 during December of YR(-1) to February of YR(0) and surface winds during September-November of YR(-1) in the tropical Indian Ocean prior to the occurrences of the 25 extreme IOD. (b) D20 and U10 (contour interval: ±0.5, ±1, ±1.5 m/s, ...) anomaly along the equator.

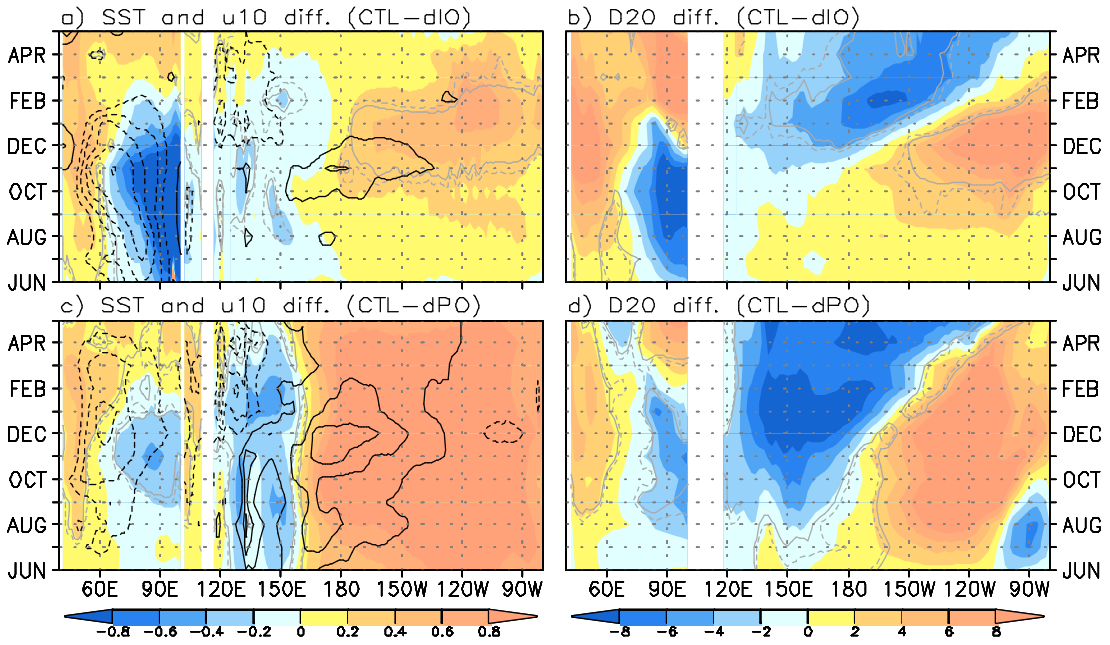

Figure 12: (a-d) Same as in Figs. 10c-f, but for the "perfect model" prediction experiments starting from 1 June of YR(0). The reduced feedback between El Niño and extreme IOD after their onsets (compared to Figs. 10c-f, see also Figs. 3 and 7) suggests the dominant role of the local Bjerknes feedback in the individual basins during the subsequent growth of these two climate modes, each of which is also subject to their intrinsic annual-phase locking (e.g., Rasmusson and Carpenter 1982; Saji et al. 1999).